THE JOURNAL OF BIOLOGICAL CHEMISTRY VOL. 285, NO. 19, pp. 14467–14474, May 7, 2010

SLC4A11 Prevents Osmotic Imbalance Leading to Corneal Endothelial Dystrophy, Deafness, and Polyuria*[S]

Received for publication, December 15, 2009, and in revised form, February 23, 2010 Published, JBC Papers in Press, February 25, 2010, DOI 10.1074/jbc.M109.094680

Nicole Gröger[‡], Henning Fröhlich[‡1], Hannes Maier[§], Andrea Olbrich[¶], Sawa Kostin[‡], Thomas Braun[‡2], and Thomas Boettger[‡3]

From the [‡]Max-Planck-Institut für Herz- und Lungenforschung, Parkstrasse 1, D-61231 Bad Nauheim, the [§]Department of Experimental Otology, Medical University of Hannover, Carl-Neuberg-Strasse 1, D-30625 Hannover, and the [¶]Department of Forest Botany and Tree Physiology, Büsgen Institute, University Goettingen, Buesgenweg 2, D-37077 Goettingen, Germany

Maintenance of ion concentration gradients is essential for the function of many organs, including the kidney, the cornea, and the inner ear. Ion concentrations and fluid content in the cornea are regulated by endothelial cells that separate the collagenous avascular corneal stroma from the anterior eye chamber. Failure to maintain correct ion concentrations leads to swelling and destruction of the cornea. In the inner ear, the stria vascularis is responsible for generating proper ion concentrations in the endolymph, which is essential for hearing. Mutations of *SLC4A11* in humans lead to syndromes associated with corneal dystrophy and perceptive deafness. The molecular mechanisms underlying these symptoms are poorly understood, impeding therapeutic interventions. The ion transporter SLC4A11 mediates sodium-dependent transport of borate as well as flux of sodium and hydroxyl ions *in vitro*. Here, we show that SLC4A11 is expressed in the endothelial cells of the cornea where it prevents severe morphological changes of the cornea caused by increased sodium chloride concentrations in the stroma. In the inner ear, SLC4A11 is located in fibrocytes underlying the stria vascularis. Loss of SLC4A11 leads to morphological changes in the fibrocytes and deafness. We demonstrate that SLC4A11 is essential for the generation of the endocochlear potential but not for regulation of potassium concentrations in the endolymph. In the kidney, SLC4A11 is expressed in the thin descending limb of Henle loop. SLC4A11 is essential for urinary concentration, suggesting that SLC4A11 participates in the countercurrent multiplication that concentrates urine in the kidney medulla.

Maintenance of extracellular salt and fluid balance is essential for every organism. Relevant structures include the mammalian kidney, essential for the regulation of body salt homeostasis. Likewise, in specific tissues the epithelia mediate fluxes of ions and water to maintain salt concentrations and electrochemical gradients. Prominent examples of such epithelia are the stria vascularis of the inner ear that generates the electrochemical driving force essential for hearing and the corneal endothelial cell layer that is essential for regulation of the fluid composition of the cornea. The ion transporter SLC4A11 was first described in 2001 (1) as a distant member of the Slc4 family of ion transporters that mediate the transport of bicarbonate, chloride, and sodium (2, 3). Based on its structural similarity to the plant borate transporter (4), a function as a mammalian borate transporter was discussed (5). Later, it was shown that SLC4A11 mediates the flux of Na^+ and OH^- into cells, although SLC4A11 can also mediate Na^+/borate cotransport in the presence of borate (6). Mutations in *SLC4A11* are associated with autosomal recessive corneal endothelial dystrophy (CHED2) (7, 8) and are also found in the Harboyen syndrome (9), a congenital corneal endothelial dystrophy associated with progressive perceptive deafness (10). It has been speculated that endothelial dystrophy and hearing loss result from improper proliferation during fetal development caused by borate-dependent effects on cell proliferation mediated via a mitogen-activated protein kinase (MAPK) pathway or by fluid imbalance in the inner ear (7). Subsequently, *SLC4A11* mutations were found in progressive degeneration of the corneal endothelium (Fuchs endothelial corneal dystrophy) (11). Some of the phenotypes observed in the human syndrome have been recently recapitulated in a mouse gene trap model of *SLC4A11*. However, the molecular mechanisms leading to the human syndromes were not addressed (12). Both the cause for progressive corneal dystrophy seen in humans patients and the possible role of borate in this process remain enigmatic (11), particularly because borate exists mostly as uncharged H_3BO_3 at physiological pH, which allows diffusion across biological membranes (6, 13). It seems more likely that *SLC4A11* is involved in the transport of fluids from the corneal endothelium to the anterior eye chamber, which counterbalances fluid "leaks" into the stroma. This endothelial fluid transport depends on transcellular HCO_3^- and Cl^- effluxes and Na^+ influx, as well as on paracellular Na^+ efflux (14). Several molecules such as NBCs, NKCC, and chloride channels are known to participate in this process, although it is likely that additional components remain to be identified (15, 16).

To address the role of SLC4A11 in endothelial ion and fluid transport and other physiological processes, we have inactivated the gene by targeted mutagenesis in the mouse. LacZ reporter and anti-SLC4A11 antibody staining (17) revealed that SLC4A11 is expressed in the endothelium of the cornea, in the

* This work was supported by the Max-Planck-Society and by Deutsche Forschungsgemeinschaft Grant BO1970/1.

[S] The on-line version of this article (available at http://www.jbc.org) contains supplemental Figs. 1and 2, Tables 1 and 2, and additional references.

[1] Present address: Inst. für Physiologie, Universität Tübingen, D-72076 Tübingen, Germany.

[2] To whom correspondence may be addressed. Tel.: 49-6032-7051102; Fax: 49-6032-7051104; E-mail: thomas.braun@mpi-bn.mpg.de.

[3] To whom correspondence may be addressed. Tel.: 49-6032-7051115; Fax: 49-6032-7051104; E-mail: thomas.boettger@mpi-bn.mpg.de.

thin descending part of Henle loop in the kidney, and in fibrocytes of the inner ear. SLC4A11 seems to play a major role at all these locations because its loss caused the following: (i) thickening of the stroma and Descement membrane concomitant with increased sodium chloride concentration in the stroma of the cornea; (ii) impaired urinary concentration, increased urinary volume, and increased urinary sodium loss in the kidney; and (iii) stress-induced morphological changes of fibrocytes of the inner ear resulting in deafness. We have uncovered the physiological basis of these phenotypes, and we propose a major role of SLC4A11 in ion homeostasis and fluid transport across various epithelial barriers.

EXPERIMENTAL PROCEDURES

Mice—A 14.8-kb SalI/PshAI *slc4a11* genomic fragment was inserted into a targeting vector containing a diphtheria toxin expression cassette. A β-galactosidase/phosphoglycerate kinase promoter-neomycin resistance expression cassette was cloned into the MluI/EcoRV sites, which resulted in a fusion of the 10th exon of SLC4A11 to the β-galactosidase coding sequence and deletion of exons 11–18 (supplemental Fig. 1). The resulting targeting vector was linearized and electroporated into MPI II embryonic stem cells (18). Genomic DNA from neomycin-resistant clones was analyzed for recombination after EcoRV digestion with a 5′ probe (662 bp), which was generated by PCR using the following primer: TCAACAAGCCAATGCTACCTGGCTC; CCCTTCCTTTCCAAGATGCAGCAGG. The WT[4] allele corresponds to 6.8 kb and the KO allele to 7.9 kb. A further 13.8-kb fragment is always present due to EcoRV cutting in the region recognized by the probe. The study was performed in a mixed 129SV/C57Bl6 background. Mice were backcrossed for two generations onto C57Bl6. All animal work was approved by the animal experiment committees of the federal state of Hessen or the City of Hamburg, Germany.

Morphology and Immunostainings—For LacZ staining, anesthetized mice were perfused through the left ventricle with PBS followed by perfusion with fixative containing 1% formaldehyde, 0.2% glutaraldehyde, 0.2% Nonidet P-40, and 0.1% deoxycholate in PBS. Tissue samples were washed in PBS and cryosectioned (see below) or stained directly in LacZ staining solution containing 2 mM $MgCl_2$, 5 mM $K_3Fe(CN)_6$, 5 mM $K_4Fe(CN)_6$, 0.2% Nonidet P-40, 0.1% deoxycholate, and 1 mg/ml 5-bromo-4-chloro-3-indolyl-β-D-galactopyranoside (X-gal, Roth) in PBS. WT animals were used as a control for staining. For histology or immunohistology, anesthetized mice were perfused with PBS followed by 4% paraformaldehyde in PBS. Adult cochleas were decalcified with Rapid Bone Decalcifier (Eurobio). Tissue samples were mounted in OCT compound (TissueTek) for cryosections or embedded in paraffin and cut into 10-μm sections. For immunostainings, cryosections were fixed in 4% paraformaldehyde, 0.1% deoxycholate, and 0.2% Nonidet P-40 in PBS, washed, and blocked in 2% bovine serum albumin, 3% goat serum, and 0.5% Nonidet P-40 in PBS. Antisera were diluted in 2% bovine serum albumin and 0.5% Nonidet P-40 in PBS. Antibodies used were anti-AE1 (1:100; Millipore; AB3500P), anti-aquaporin-1 (1:100; Alpha Diagnostic; AQP11-A), anti-calbindin (1:100; Abcam; ab25085); anti-Tamm Horsfall Protein (1:100; Biodesign International; K90071C), and phalloidin-TRITC (1:1000, Sigma; P-1951). Secondary antibodies and TOTO-3 were from Invitrogen. Anti-SLC4A11 antiserum (1:200) was a gift from J. Praetorius (17). Analysis was performed using an Axiophot microscope (Zeiss) or by confocal microscopy (Leica). For electron microscopy, eyes were fixed in 2.5% glutaraldehyde for 12 h at 40 °C and embedded in Epon. Inner ears were collected after perfusion of animals using PBS solution via the heart apex at 100 mm Hg pressure for 2 min, followed by perfusion with 4% paraformaldehyde in PBS. Cochleas were dissected and additionally fixed in 2.5% glutaraldehyde for another 12 h at 40 °C, decalcified in 10% EDTA for 7 days, and embedded in Epon. Ultrathin sections were stained with uranyl acetate and lead citrate, viewed, and photographically recorded using a Philips CM 10 electron microscope.

EDX Analysis—X-ray microanalysis was performed as described previously (19). In brief, eyes were rapidly removed from mice after sacrifice and frozen in a mixture of propane/isopentane (2:1) at the temperature of liquid nitrogen. Samples were infiltrated with ether after freeze-drying, embedded in styrene-methacrylate, and cut into 2-μm sections with an Ultramicrotome. EDX was done with STEM TECNAI-G^2 Spirit BioTwin (FEI). X-rays were detected with the EDX detector (EDAX) at 80 kV. Data were analyzed using the TIA imaging and analysis software by FEI. Kα line peak area intensities (counts) of the measuring positions located in the corneal endothelium and stroma from several points were calculated und used for further statistical analysis.

Auditory-evoked Brain Stem Response Hearing Thresholds—Auditory-evoked brain stem responses to clicks were recorded in anesthetized animals (16 mg/kg xylazine hydrochloride, 60 mg/kg *S*-ketamine hydrochloride) on a heating pad in a soundproof chamber. Acoustic click stimuli were delivered monoaurally using a Beyer DT-48 earphone and were monitored with a probe microphone (MK301, Microtech Gefell) integrated into the earpiece. Bioelectric potentials were recorded by subcutaneous silver electrodes at the vertex (reference), forehead (ground), and ventrolateral to the stimulated ear, and alternating clicks (~200-μs duration) were applied at a rate of 21/s and averaged 400–2000 times. Stimulus intensities were varied, starting at 118-db peak equivalent SPL (db SPL pe) in increments of 20 db except near threshold where 5-db steps were used. The hearing threshold was defined as the lowest intensity to generate a reproducible auditory-evoked brain stem response wave forms.

Endocochlear Potential and Endolymph Potassium—Measurements of endocochlear potential (EP) and potassium concentration ($[K^+]$) were performed in anesthetized mice (14 mg/kg xylazine hydrochloride, 40 mg/kg *S*-ketamine hydrochloride) on a heated surgical table. The bulla was opened laterally, leaving the tympanic membrane intact, and the bone over the 1st turn of the cochlea was thinned and opened below the stapedial artery. A single (EP) or double-barreled ($[K^+]$)

[4] The abbreviations used are: WT, wild type; PBS, phosphate-buffered saline; KO, knock-out; TRITC, tetramethylrhodamine isothiocyanate; EDX, energy-dispersive x-ray spectroscopy; EP, endocochlear potential.

microelectrode was inserted, and voltage and K^+ potentials were measured against an Ag/AgCl reference electrode under the skin on the neck of the animal. K^+-selective barrels contained liquid K^+ ionophores (Fluka, 60398) and were calibrated before and after experiments. For details see Ref. 20.

RESULTS

slc4a11 knock-out mice were generated by inserting a β-galactosidase coding sequence in-frame into the 10th exon of *slc4a11* (supplemental Fig. 1). This mutation leads to the truncation of the SLC4A11 protein before the first predicted transmembrane domain resulting in a cytoplasmic localization of the β-galactosidase fusion protein *in vivo*. Breeding of homozygous *slc4a11* mutant mice did not reveal gross morphological malformation. Mutant mice were fertile and showed a normal weight and life span.

SLC4A11 Is Expressed in the Endothelial Cells of the Cornea, and Loss of SLC4A11 Leads to Severe Morphological Alterations—Analysis of the expression of the *lacZ* gene inserted into the *slc4a11* locus revealed β-galactosidase staining specifically in endothelial cells but not epithelial cells of the cornea (Fig. 1*A*). Localization of lacZ activity matched the expression of the SLC4A11 protein in endothelial cells of the cornea as shown by immunofluorescence (Fig. 1*B*) using an antibody described previously (17). Specificity of the antibody is demonstrated using knock-out tissue (Fig. 1*C*). Morphological analysis of the cornea of SLC4A11 mutant mice revealed morphological alterations in all layers of the cornea of 12-month-old mice (Fig. 1, *D* and *E*). The endothelial cell layer, which is the sole corneal cell layer that expresses SLC4A11, was thickened in the KO animals (KO, 4.5 ± 0.1 μm; WT, 2.2 ± 0.1 μm; $n = 3/3$ animals; $p < 0.001$; Fig. 1, *F* and *G*). We also observed numerous intracellular vacuolation in the endothelial cell layer indicating disturbance of osmotic balance of the endothelial cells. Furthermore, we detected a thickening of the Descement membrane (KO, 4.6 ± 0.4 μm; WT, 2.4 ± 0.1 μm; $n = 3/3$ animals, $p < 0.01$) and of the corneal stroma (KO, 167.7 ± 12.7 μm; WT, 87.7 ± 5.4 μm; $n = 4/3$ animals, $p < 0.005$). The corneal epithelium was also thickened (KO, 47.8 ± 3.8 μm; WT, 30.3 ± 4.3 μm; $n = 4/3$ animals, $p < 0.05$) and characterized by loss of the typical cuboidal shape of cells at the basal membrane and of flat cells at the surface. The analysis of the morphological changes revealed more severe changes than observed in a previous study using an *slc4a11* gene trap mutation (12). It is unclear whether the less severe phenotype described previously might be due to incomplete disruption of Slc4a11 by the gene trap mutation (21, 22) or due to differences in the pathological stages analyzed.

Formation of NaCl Crystals in the Cornea of SLC4A11 Mutant Mice Demonstrates Malfunctions in Ion Homeostasis—Because SLC4A11 has been proposed to act as an ion transporter, we investigated a possible accumulation of inorganic salts in the cornea of SLC4A11 mutants using EDX. In flash-frozen sections of knock-out mutants, we observed crystals that were not observed in WT animals (Fig. 2, *A* and *B*, *arrows*; 4 KO/4 WT animals). EDX analysis revealed that these crystals always consisted of sodium chloride (Fig. 2*G*). In addition, we found a dramatic increase in sodium and chlorine concentrations in the corneal stroma (based on peak area intensity for the sodium and chlorine Kα line, sodium: KO, 153 ± 44 counts; WT, 50 ± 25 counts, $n = 4/4$ animals; $p < 0.05$; chlorine: KO, 183 ± 38 counts; WT, 60 ± 32 counts, $n = 4/4$ animals; $p < 0.03$; Fig. 2, *A–D* and *H*). Sodium concentration was also increased in knock-out compared with WT endothelial cells (peak area intensity for sodium Kα line: KO, 68 ± 11; WT, 37 ± 2 counts; $n = 4/4$ animals; $p < 0.02$, Fig. 2, *A, B, E, F,* and *H*), whereas chlorine concentrations were not changed consistently. For comparison, EDX analysis of sodium chloride crystals was performed sodium chloride crystals in KO mice: sodium 1974 ± 332 counts; chlorine, 2211 ± 418 counts, 10 crystals from four KO mice).

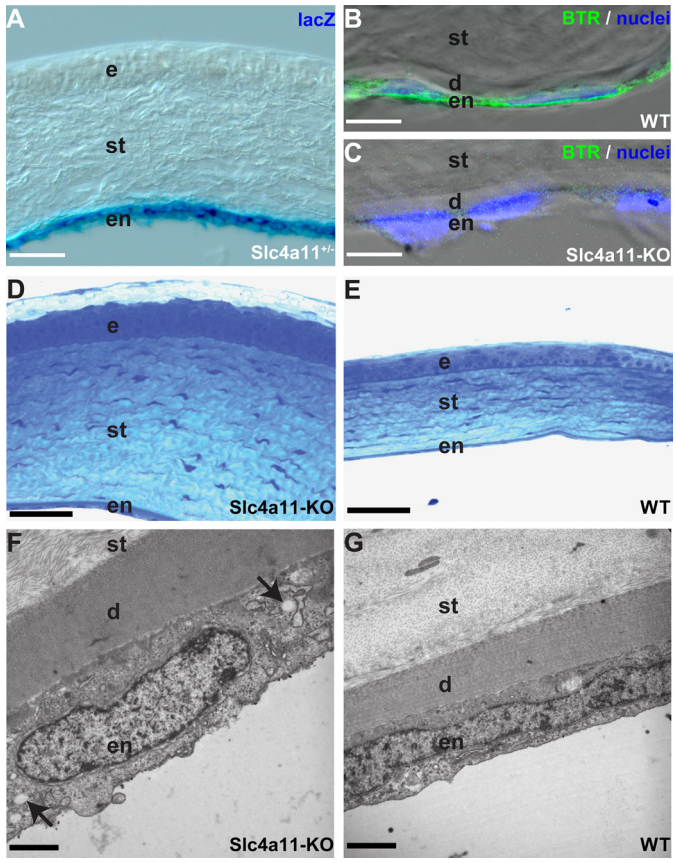

FIGURE 1. **Loss of SLC4A11 in endothelial cells leads to morphological alterations of the cornea.** SLC4A11 is expressed in endothelial cells of the cornea (*A* and *B*). LacZ fusion protein expression (*blue*) in heterozygous animals (*A*) and antibody staining (*green*) in WT animals (*B*) reveals expression of SLC4A11 in the endothelium of the cornea. Antibody staining of KO tissue (*C*) proves specificity of the antibody. Nuclei in *B* and *C* are stained with TOTO-3 (*blue*). Sections through the cornea of *slc4a11* knock-out (*D*) and WT mice (*E*) clearly reveal a significant thickening of the corneal stroma with disturbance of the stratification of the epithelium. Electron microscopy sections reveal a thickened Descement membrane and enlarged endothelial cells in *slc4a11* knock-out (*F*) compared with WT mice (*G*). Note intracellular vacuolation (*arrows* in *F*) in the endothelial cells of KO animals. *d*, Descement's membrane; *e*, epithelium; *en*, endothelium; *st*, stroma. *Scale bars* used are as follows: *A*, 87 μm; *B* and *C*, 7 μm; *D* and *E*, 50 μm; *F* and *G*, 2 μm.

SLC4A11 Is Expressed in the Thin Descending Limb of Henle Loop—In the kidney, expression of SLC4A11 was detected by LacZ and antibody staining (Fig. 3, *A–H*). Expression of SLC4A11 localized to the kidney medulla (Fig. 3*A*). Here, SLC4A11-LacZ was co-localized with the expression of aquaporin-1 (Fig. 3, *B–D*). Aquaporin-1 is located in the proximal

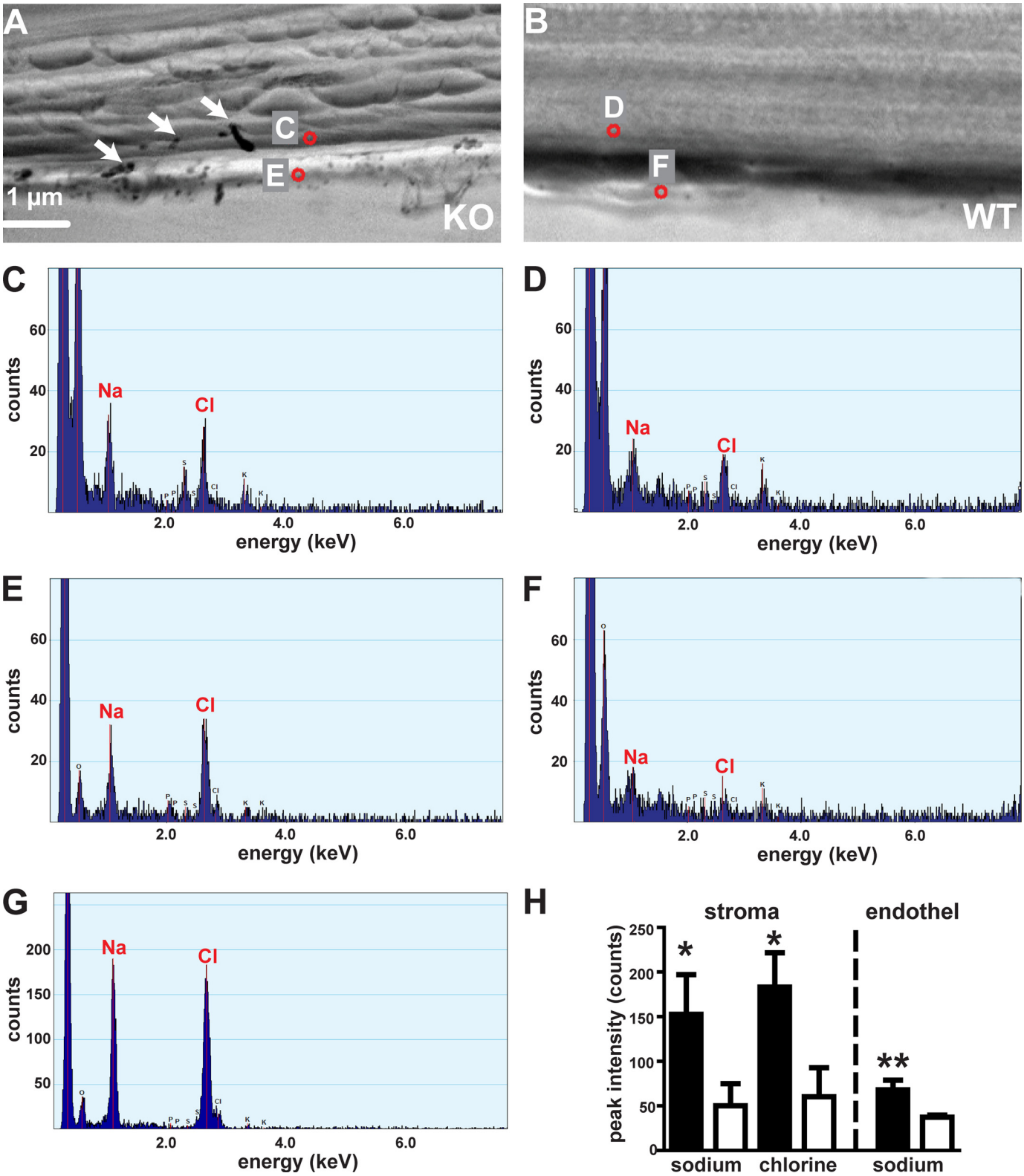

FIGURE 2. **Increased salt concentration in the cornea of SLC4A11 mutant mice.** An EDX analysis of KO (*A*) and WT (*B*) corneal sections was performed at different positions within the cornea. Locations of example spots (*red circles*) are indicated in *A* and *B*; marked spots correspond to respective spectra in *C–F*. *Arrows* in *A* mark sodium chloride crystals found only in KO cornea. Crystal composition was characterized by EDX analysis, and sodium crystals were excluded from further analysis. Representative spectra are shown for stromal (*C* and *D*) and endothelial cells (*E* and *F*) of KO (*C* and *E*) and WT (*D* and *F*) cornea. The spectrum of a sodium chloride crystal is shown in *G*. Note the different *y* axis scale. Statistical analysis of element specific Kα line peaks reveal significant increase of sodium (Na) and chlorine (Cl) in the stroma of mutant corneas (*H*). Only the sodium concentration is significantly increased in endothelial cells of mutants (*H*). *Filled bars*, mutants; *open bars*, WT; *, $p < 0.05$; **, $p < 0.02$.

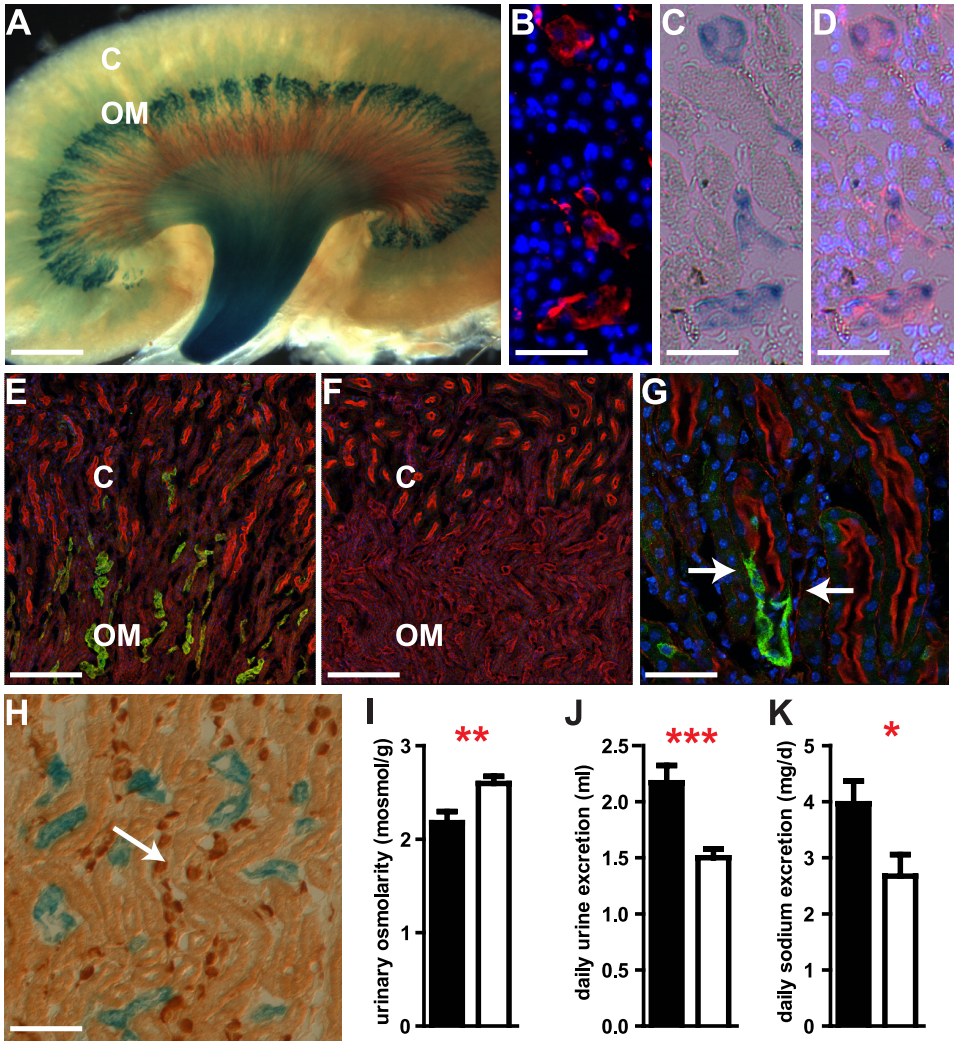

FIGURE 3. **SLC4A11 in the thin descending limb of Henle loop is essential for urinary concentration.** SLC4A11-LacZ fusion protein is localized (*blue*) in the medulla of the kidney (*A*). The expression of tubular aquaporin-1 (*red, B*) and of SLC4A11-LacZ (*C, blue*) co-localizes (*D*) in the medulla of the kidney. Nuclei are stained with TOTO-3 (*blue*; *B, C,* and *G*). SLC4A11 protein is detected in the medulla of the WT kidney (*E* and *G*; *green*), which coincides with the activity of SLC4A11-LacZ. SLC4A11 protein (*green*) is not present in proximal tubules (*E* and *G*) marked by staining of the brush border by phalloidin (*red*). SLC4A11 protein is absent in kidneys of KO animals (*F*). Localization of SLC4A11 protein (*green*) in the thin descending part of Henle loop close to the junction of the proximal tubule (marked by phalloidin staining in *red*) is shown in *G* (junction marked by *arrows*). Expression of SLC4A11-LacZ (*blue*) is not found in the collecting duct marked by AE1 staining (*H*; *brown, arrow*). Similarly, SLC4A11 is not detected in thick ascending limb and connecting tubule (see text). Loss of SLC4A11 leads to reduced urinary osmolarity (*I*) and increased daily urine (*J*) and sodium excretion (*K*) indicating defects in fluid resorption in the kidney (*filled bars*, mutants; *open bars*, WT; ***, $p < 0.001$; **, $p < 0.01$; *, $p < 0.05$; *C*, kidney cortex; *OM*, outer medulla; *scale bars* used are as follows: *A*, 1.2 mm; *B* and *C*, 43 μm; *E* and *F*, 174 μm; *G*, 43 μm; *H*, 100 μm).

TABLE 1

Analysis of urinary ion secretion per day in WT and *slc4a11* knock-out mice

Urine was collected daily using metabolic cages. Note the increased total urinary secretion of sodium, chloride, potassium, and magnesium in the KO mice.

	KO	WT	*n* (WT/KO)	*p* value
Sodium (mg/day)	3.96 ± 0.4	2.67 ± 0.38	10/10	0.032
Chloride (mg/day)	14.42 ± 1.12	11.69 ± 0.3	9/10	0.039
Potassium (mg/day)	27.62 ± 1.7	22.8 ± 1.17	7/9	0.045
Magnesium (mg/day)	1.11 ± 0.12	0.81 ± 0.07	10/10	0.047
Calcium (mg/day)	0.19 ± 0.02	0.22 ± 0.02	10/10	0.408
Inorganic phosphate (mg/day)	3.11 ± 0.58	4.29 ± 1.12	10/10	0.361

tubule and in the descending thin limb of long loop nephrons and is essential for urinary concentration (23–25). SLC4A11 was not expressed in proximal tubule cells, which were identified by brush border staining with phalloidin-TRITC (Fig. 3, *E–G*). However, we specifically observed SLC4A11 expression at the cortex-medulla border in the thin descending loop, which follows the proximal tubule and lacks a brush border (Fig. 3*G*). No expression of SLC4A11 was found in the thick ascending limb, in the connecting tubule, or the collecting duct (Fig. 3*H*), which were identified by anti-Tamm Horsfall protein, anti-calbindin, and anti-AE1 staining, respectively. We conclude that SLC4A11 expression in the kidney is confined to the thin descending limb of Henle loop. Specificity of the anti-SLC4A11 antiserum was demonstrated in kidney sections from knock-out animal by the absence of specific staining (Fig. 3*F*).

SLC4A11 Mutant Mice Suffer from Polyuria, Loss of NaCl, and Hypo-osmolarity of the Urine—Analysis of kidney function in *slc4a11* knock-out mice revealed multiple defects consistent with expression pattern of SLC4A11 in the water transporting thin descending parts of Henle loops. The urine of knock-out mice collected in metabolic cages had a reduced osmolarity (KO, 2178 ± 118 mosmol/kg; WT, 2597 ± 76 mosmol/kg; $n = 9/8$ animals; $p = 0.01$; Fig. 3*I*). Moreover, we found a larger urinary volume (KO, 2.2 ± 0.15 ml; WT, 1.5 ± 0.1 ml, $n = 10/10$ animals; $p = 0.001$; Fig. 3*J*) and a reduction of the urinary concentration of calcium in knock-out animals (supplemental Table 1). Calculation of the daily secretion of ions revealed an increased urinary loss of sodium (Fig. 3*K*), chloride, potassium, and magnesium in the *slc4a11* knock-out animals (Table 1). However, the sodium concentrations in urine did not change significantly (supplemental Table 1). To characterize possible secondary changes, which might have arisen from counter-regulatory processes in the kidney after chronic loss of SLC4A11 function, we conducted a comprehensive microarray analysis. We did not observe transcriptional changes of genes known to be involved in the mechanisms of urinary concentration (26) such as different aquaporins, NHE3, NKCC2, ROMK, ClC-Ks, ENACs, or urate transporters (supplemental Table 2). This suggests that the changes in urine composition were directly caused by the absence of SLC4A11. The minimum information about a microarray

experiment-compliant microarray data is available at Array Express.

Loss of SLC4A11 Leads to Vacuolation of Fibrocytes Underlying the Stria Vascularis of the Cochlea—In the inner ear, antibody and LacZ staining marked type I, II, and IV fibrocytes, which underlie the stria vascularis (Fig. 4, *A* and *B*). We did not observe a gross morphological change of the cochlea in *slc4a11* knock-out mice nor a change of the total number of fibrocytes in animals up to 6 months of age (Fig. 4, *C* and *D*). Quantification of fibrocytes in hematoxylin and eosin-stained sections of the cochlea failed to reveal changes in the number of fibrocytes (KO, 197.0 ± 6.4; WT, 188.0 ± 3.0 fibrocyte-nuclei/section, $n = 6/7$ animals; calculated from the mean of three sections/animal). Interestingly, we observed severe disruptions of the typical morphology of fibrocytes in the *slc4a11* knock-out mice by electron microscopy. *slc4a11* KO fibrocytes were characterized by numerous intracellular vacuolations and extracellular edemas indicating disturbance of the osmotic balance of these cells (Fig. 4, *E* and *F*).

Impaired Hearing in slc4a11 Knock-out Mice Is Associated with Loss of Endocochlear Potential but Preserved Potassium Concentration in the Endolymph—To complete our phenotypic characterization of *slc4a11* knock-out mice, we recorded auditory click evoked brainstem responses. We observed a reduced hearing threshold in knock-out animals at 3 weeks of age (KO, 79.6 ± 3.3 db; WT, 22.0 ± 2.6 db; $n = 12/10$ animals; $p < 0.001$) that persisted in 3-month-old animals (KO, 87.1 ± 4.0 db; WT, 23.8 ± 9.8 db; $n = 14/14$ animals, $p < 0.001$; Fig. 4*G*). Next, we measured the endocochlear potential and the potassium concentration of the endolymph to investigate the molecular basis of the observed hearing deficit (Fig. 4, *H–J*). The endocochlear potential was strongly reduced in *slc4a11* knock-out animals compared with WT animals (KO, 42.9 ± 2.6 mV; WT, 111.3 ±

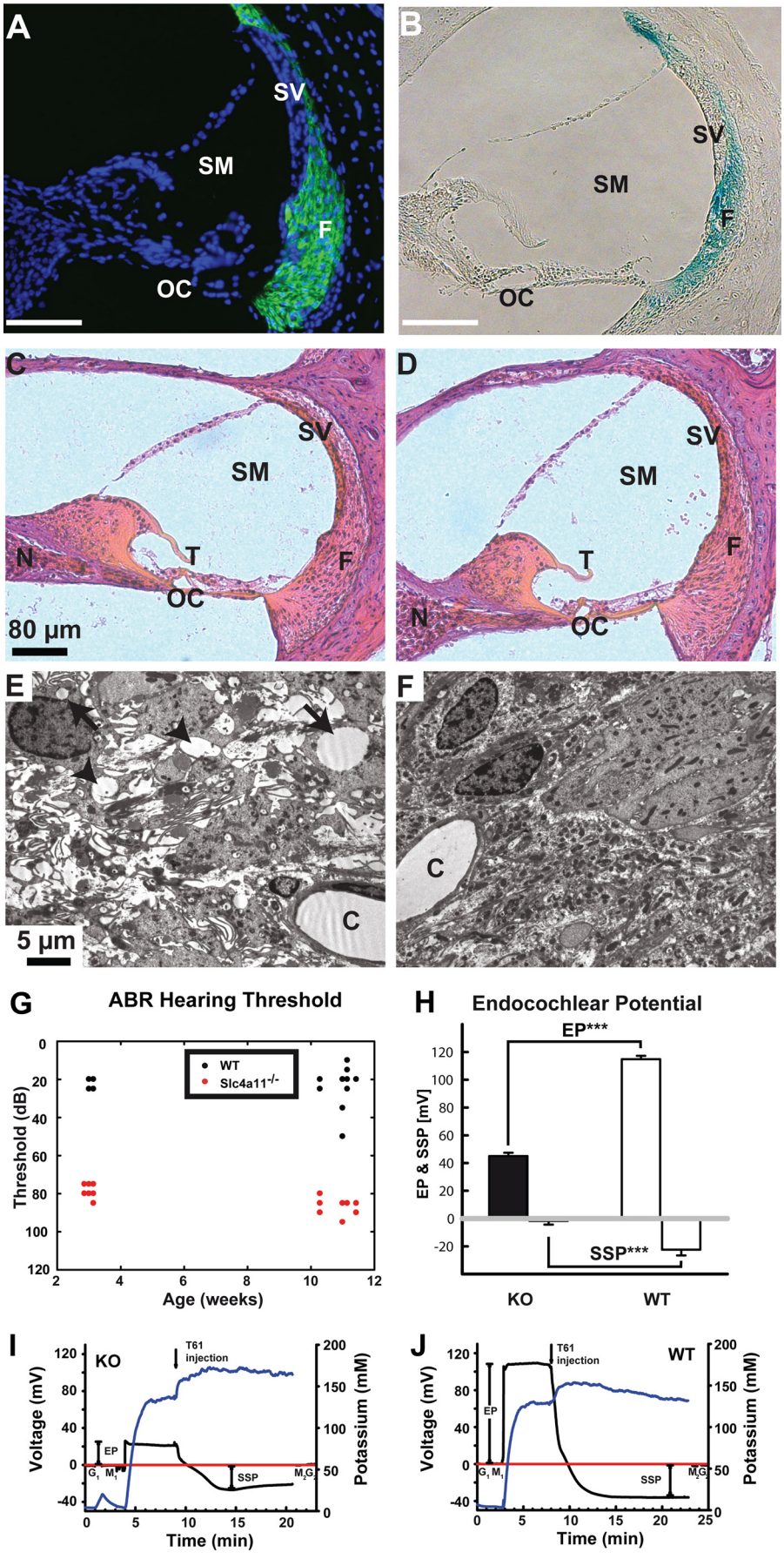

2.9 mV; $n = 8/7$ animals; $p < 0.001$; Fig. 4*H*). In addition, the steady state potential was strongly reduced in *slc4a11* knock-out animals (KO, 2.8 ± 2.6 mV; WT, −24.3 ± 3.7 mV; $n = 8/7$ animals; $p < 0.001$; Fig. 4*H*). To differentiate between effects of the *slc4a11* knock-out on EP and potassium concentration, we measured the potassium concentration in the scala media of adult *slc4a11* knock-out and WT animals. No difference in the potassium concentration was found (KO, 135.7 ± 2.3 mM; WT, 139.4 ± 5.5 mM, $n = 3/3$ animals, $p > 0.56$; Fig. 4, *I* and *J*) suggesting that the hearing deficit was caused by reduction of the EP.

SLC4A11 Mutations Found in Humans Lead to Changes in Subcellular Localization—To investigate the molecular pathogenesis caused by SLC4A11 human variants, we analyzed the cellular localization of two mutant SLC4A11 proteins found in human patients. Expression of the CHED2 A269V point mutation and the F672del deletion (27, 28) in Madin-Darby canine kidney epithelial cells resulted in aberrant subcellular localizations. Both mutant proteins resided in the cytoplasm and did not demonstrate the typical membrane localization characteristic for wild type SLC4A11 (supplemental Fig. 2). Our results suggest that the phenotype of the human syndromes is caused by the absence of SLC4A11 from the plasma membrane and not necessarily from changes in the transport properties of SLC4A11.

DISCUSSION

Mutations of *SLC4A11* in humans lead to syndromes that are regularly associated with corneal dystrophy and variable other phenotypic changes. Previous studies indicated that some of the disease-causing mutations in humans lead to the loss of membrane localization of the transporter (11), which would likely affect the ion transport function of SLC4A11. Similarly, the disease-causing mutations of SLC4A11 A269V (28) and F672del (27) also cause the mislocalization of SLC4A11 with an accumulation in intracellular compartments. It has been suggested that the CHED phenotype is due to the loss of borate transport, leading to a borate deficiency that impacts the proliferation and maintenance of SLC4A11-expressing cells (7). This hypothesis suffers from two major flaws. (i) It is unclear why only certain cells in the cornea and inner ear might require a borate transport. (ii) Borate can pass biological membranes as an uncharged molecule at physiological pH, which alleviates the need for a specific borate transporter (13). However, it is well known that the cornea and inner ear depend critically on an extremely tightly controlled fluid and ion transport. Hence, it seems likely that the loss of sodium flux, mediated by SLC4A11, is responsible for CHED (10). Here, we clearly demonstrate that endothelial cells of the cornea or fibrocytes of the inner ear of *slc4a11* knock-out mice do not suffer from reduced proliferation or an increased rate of cell death but from enrichment of sodium in distinct cell types. We have presented evidence that sodium chloride accumulates in the corneal stroma, although increased sodium concentrations were found in endothelial cells. Because sodium transport is essential for the directional transport of fluid in the cornea (14, 29) and SLC4A11 can act as a sodium channel (6), it is likely that its loss disrupts the intricate balance of the flux of fluids through the endothelium (15). Disturbance of ion gradients will lead to accumulation of sodium chloride in the corneal stroma and collection of water in the normally dehydrated cornea.

A similar situation might exist in the kidney, which is the main organ regulating the secretion of water and solutes from the body. An essential part of the function of the kidney is to concentrate urine to limit the loss of water from the body. This ability critically depends on the presence of hyperosmolar concentrations of sodium chloride in the renal medullary interstitium, which are generated by countercurrent multiplication (30, 31 and reviewed in Ref. 32). Henle loop plays a major role in this process, which creates the hyperosmolarity by concentrating solutes in the medullary interstitium. The medullary ascending part of the Henle loop actively transports NaCl from the lumen to the interstitium, whereas the water is retained in the lumen of the ascending loop due to low water permeability. This dilution of the luminal fluid in the ascending limb generates a transepithelial osmolarity difference that is multiplied by countercurrent multiplication between the two parts of the Henle loop and thus results in the large osmotic gradient along the loop of Henle. For this effect, it is essential that the luminal fluid along the descending loop is close to osmotic equilibrium, which is achieved by outward flux of water from the descending loop, mainly mediated by aquaporin-1 (23, 33–35). Importantly, the influx of sodium chloride into the descending loop contributes to increased luminal and interstitial osmolarity along the descending loop (36). So far, the molecular basis of this sodium flux in the descending thin loop was not known. Here, we show that loss of SLC4A11 from the cells of the thin descending loops of the kidney leads to decreased urinary osmolarity with increased urinary volume und increased sodium excretion by SLC4A11 mutant mice. This finding clearly defines a role of SLC4A11 for mediating a sodium flux into the thin descending

FIGURE 4. **Morphological alterations in the inner ear, impaired hearing, and loss of the endocochlear potential but preserved endolymph potassium concentration in SLC4A11 mutant mice.** Anti-SLC4A11 antibody staining (*green*) in WT animals (*A*) reveals expression of SLC4A11 in the fibrocytes of the cochlea. Nuclei are stained with TOTO-3 (*blue*). LacZ fusion protein expression (*blue*) in heterozygous animals (*B*) confirms expression in fibrocytes. Hematoxylin and eosin-stained sections through the inner ear of *slc4a11* knock-out (*C*) and WT mice (*D*) reveal no morphological changes at the light microscopy level. Electron microscopy images uncover abnormal cellular structures of fibrocytes in the stria vascularis of mutant (*E*) mice compared with WT (*F*), which are characterized by extracellular edema (*arrowheads*) and intracellular vacuolation (*arrows*). Measurement of hearing thresholds in KO and WT mice by auditory-evoked brain stem responses to clicks was recorded in anesthetized mice (*G*). Note the significantly reduced hearing threshold in KO mice at 3 weeks of age and in the older animals. *H–J,* strongly reduced endocochlear potential in KO mice compared with WT mice in the presence of normal potassium concentrations in the scala media. Representative measurements with combined EP (*black line*) and potassium recordings (*blue line*) are shown in *I* and *J*. The reference potential (*red line*) was recorded before the experiment in tissue (G_1) and in the fluid meniscus (M_1) overlying the cochlear opening. The reference potential was controlled at the same sites subsequent to the experiment (M_2 and G_2). Animals were sacrificed during endocochlear recording (T61 injection, Intervet), which causes an immediate loss of the endocochlear potential with subsequent formation of a passive steady state potential. *C,* capillaries; *EP,* endocochlear potential; *F,* fibrocytes; *N,* neurons; *OC,* organ of corti; *SM,* scala media; *SSP,* steady state potential; *SV,* stria vascularis; *T,* tectorial membrane; ***, $p < 0.001$.

limb of Henle loop to allow countercurrent multiplication by osmotic equilibration.

Endothelial cells of the corneal stroma and the thin descending part of the Henle loop are both fluid leaky epithelia, which express aquaporin-1 and SLC4A11 and achieve sodium transport under near iso-osmotic conditions. Although the function of both organs differs significantly, some physiological processes, *i.e.* the regulation of extracellular fluid volume (Henle loop) and the generation of hydrostatically driven flow into the stroma along with the establishment of opposing ion gradients to maintain the relatively dehydrated corneal stroma, resemble each other and appear to be mediated by the same molecule.

Our analysis of the inner ear phenotype suggests a mechanism to explain the hearing loss in SLC4A11 mutants. We demonstrated a reduction of the endocochlear potential of the inner ear. The endocochlear potential is essential for the function of the (outer) hair cells of the inner ear. We suggest that the impaired endocochlear function is the molecular cause of the hearing loss in mice and most likely also in humans. SLC4A11 mutant mice are characterized by phenotypic changes within fibrocytes, although the total cell number does not change. The fibrocyte layer underlying the stria vascularis encircles the stria vascularis and provides the only path for potassium recycling. Our results demonstrate that SLC4A11 is involved in transport of potassium through the fibrocyte layer to the stria vascularis. Most likely, the reduced supply of potassium into the stria vascularis leads to decreased potassium secretion by intermediate cells of the stria vascularis, which are essential for generation of the electric potential of the inner ear. The reduction of the endocochlear potential disables outer hair cells to amplify auditory signal. However, the remaining endocochlear potential and the high potassium concentration still allow survival of outer hair cells. Interestingly, the potassium concentrations in the endolymph are not affected by the reduced supply to the stria, probably because marginal cells of the stria are not as severely affected by the reduced fibrocyte function as intermediate cells. The maintenance of a normal potassium concentration might also be supported by the reduced potassium drain from the endolymph when outer hair cells lose their function. Taken together, our studies have uncovered a critical function of Slc4a11 in sodium-mediated fluid transport in different organs, which, although they have different functions, rely on related physiological processes mediated by SLC4A11 to accomplish similar biophysical tasks.

Acknowledgments—We thank Sylvia Thomas, Ulrike Neckmann, and Ulli Schlapp for technical support and Jeppe Prætorius for the SLC4A11 antiserum. We thank Matthew Wheeler for discussion of the manuscript. H. M. thanks Andrej Kral (Medical University Hannover) for providing the opportunity to work in his laboratory. We thank Andrea Polle (University of Göttingen) for help with EDX analysis.

REFERENCES

1. Parker, M. D., Ourmozdi, E. P., and Tanner, M. J. (2001) *Biochem. Biophys. Res. Commun.* **282,** 1103–1109
2. Pushkin, A., and Kurtz, I. (2006) *Am. J. Physiol. Renal Physiol.* **290,** F580–F599
3. Romero, M. F. (2005) *Curr. Opin. Nephrol. Hypertens.* **14,** 495–501
4. Takano, J., Noguchi, K., Yasumori, M., Kobayashi, M., Gajdos, Z., Miwa, K., Hayashi, H., Yoneyama, T., and Fujiwara, T. (2002) *Nature* **420,** 337–340
5. Frommer, W. B., and von Wirén, N. (2002) *Nature* **420,** 282–283
6. Park, M., Li, Q., Shcheynikov, N., Zeng, W., and Muallem, S. (2004) *Mol. Cell* **16,** 331–341
7. Vithana, E. N., Morgan, P., Sundaresan, P., Ebenezer, N. D., Tan, D. T., Mohamed, M. D., Anand, S., Khine, K. O., Venkataraman, D., Yong, V. H., Salto-Tellez, M., Venkatraman, A., Guo, K., Hemadevi, B., Srinivasan, M., Prajna, V., Khine, M., Casey, J. R., Inglehearn, C. F., and Aung, T. (2006) *Nat. Genet.* **38,** 755–757
8. Aldave, A. J., Yellore, V. S., Bourla, N., Momi, R. S., Khan, M. A., Salem, A. K., Rayner, S. A., Glasgow, B. J., and Kurtz, I. (2007) *Cornea* **26,** 896–900
9. Harboyan, G., Mamo, J., Kaloustian, V., and der Karam, F. (1971) *Arch. Ophthalmol.* **85,** 27–32
10. Desir, J., Moya, G., Reish, O., Van Regemorter, N., Deconinck, H., David, K. L., Meire, F. M., and Abramowicz, M. J. (2007) *J. Med. Genet.* **44,** 322–326
11. Vithana, E. N., Morgan, P. E., Ramprasad, V., Tan, D. T., Yong, V. H., Venkataraman, D., Venkatraman, A., Yam, G. H., Nagasamy, S., Law, R. W., Rajagopal, R., Pang, C. P., Kumaramanickevel, G., Casey, J. R., and Aung, T. (2008) *Hum. Mol. Genet.* **17,** 656–666
12. Lopez, I. A., Rosenblatt, M. I., Kim, C., Galbraith, G. C., Jones, S. M., Kao, L., Newman, D., Liu, W., Yeh, S., Pushkin, A., Abuladze, N., and Kurtz, I. (2009) *J. Biol. Chem.* **284,** 26882–26896
13. Dordas, C., and Brown, P. H. (2001) *Biol. Trace Elem. Res.* **81,** 127–139
14. Diecke, F. P., Ma, L., Iserovich, P., and Fischbarg, J. (2007) *Biochim. Biophys. Acta* **1768,** 2043–2048
15. Bonanno, J. A. (2003) *Prog. Retin. Eye Res.* **22,** 69–94
16. Fischbarg, J., Diecke, F. P., Iserovich, P., and Rubashkin, A. (2006) *J. Membr. Biol.* **210,** 117–130
17. Damkier, H. H., Nielsen, S., and Praetorius, J. (2007) *Am. J. Physiol. Regul. Integr. Comp. Physiol.* **293,** R2136–R2146
18. Voss, A. K., Thomas, T., and Gruss, P. (1997) *Exp. Cell Res.* **230,** 45–49
19. Fritz, E. (2007) *Microsc. Microanal.* **13,** 233–244
20. Rickheit, G., Maier, H., Strenzke, N., Andreescu, C. E., De Zeeuw, C. I., Muenscher, A., Zdebik, A. A., and Jentsch, T. J. (2008) *EMBO J.* **27,** 2907–2917
21. Lee, T., Shah, C., and Xu, E. Y. (2007) *Mol. Hum. Reprod.* **13,** 771–779
22. Skarnes, W. C. (2005) *Proc. Natl. Acad. Sci. U.S.A.* **102,** 13001–13002
23. Chou, C. L., Knepper, M. A., Hoek, A. N., Brown, D., Yang, B., Ma, T., and Verkman, A. S. (1999) *J. Clin. Invest.* **103,** 491–496
24. Nielsen, S., Frøkiaer, J., Marples, D., Kwon, T. H., Agre, P., and Knepper, M. A. (2002) *Physiol. Rev.* **82,** 205–244
25. Zhai, X. Y., Fenton, R. A., Andreasen, A., Thomsen, J. S., and Christensen, E. I. (2007) *J. Am. Soc. Nephrol.* **18,** 2937–2944
26. Morris, R. G., Uchida, S., Brooks, H., Knepper, M. A., and Chou, C. L. (2005) *Am. J. Physiol. Renal Physiol.* **289,** F194–F199
27. Ramprasad, V. L., Ebenezer, N. D., Aung, T., Rajagopal, R., Yong, V. H., Tuft, S. J., Viswanathan, D., El-Ashry, M. F., Liskova, P., Tan, D. T., Bhattacharya, S. S., Kumaramanickavel, G., and Vithana, E. N. (2007) *Hum. Mutat.* **28,** 522–523
28. Hemadevi, B., Veitia, R. A., Srinivasan, M., Arunkumar, J., Prajna, N. V., Lesaffre, C., and Sundaresan, P. (2008) *Arch. Ophthalmol.* **126,** 700–708
29. Bonanno, J. A., and Giasson, C. (1992) *Invest. Ophthalmol. Vis. Sci.* **33,** 3058–3067
30. Wirz, H., Hargitay, B., and Kuhn, W. (1951) *Helv. Physiol. Pharmacol. Acta* **9,** 196–207
31. Kuhn, W., and Ramel, A. (1959) *Helv. Chim. Acta* **42,** 628–660
32. Fenton, R. A., and Knepper, M. A. (2007) *Physiol. Rev.* **87,** 1083–1112
33. Nielsen, S., Pallone, T., Smith, B. L., Christensen, E. I., Agre, P., and Maunsbach, A. B. (1995) *Am. J. Physiol.* **268,** F1023–F1037
34. Ma, T., Yang, B., Gillespie, A., Carlson, E. J., Epstein, C. J., and Verkman, A. S. (1998) *J. Biol. Chem.* **273,** 4296–4299
35. Schnermann, J., Chou, C. L., Ma, T., Traynor, T., Knepper, M. A., and Verkman, A. S. (1998) *Proc. Natl. Acad. Sci. U.S.A.* **95,** 9660–9664
36. Jamison, R. L., Buerkert, J., and Lacy, F. (1973) *Am. J. Physiol.* **224,** 180–185